# Downconversion for solar cells in $YF_3:Nd^{3+}$, $Yb^{3+}$

Janne-Mieke Meijer,[1] Linda Aarts,[1] Bryan M. van der Ende,[1] Thijs J. H. Vlugt,[2] and Andries Meijerink[1,*]
[1]*Condensed Matter and Interfaces, Debye Institute for Nanomaterials Science, Utrecht University, Princetonplein 5, 3584 CC Utrecht, The Netherlands*
[2]*Process & Energy Laboratory, Delft University of Technology, Leeghwaterstraat 44, 2628 CA Delft, The Netherlands*
(Received 9 October 2009; published 12 January 2010)

Energy losses inherent to the conversion of sunlight to electricity in solar cells are mainly due to the so-called spectral mismatch: low energy photons are not absorbed while the energy of high energy photons is only partly used by the solar cell. The losses can be significantly reduced by adapting the solar spectrum. A promising avenue is the use of a downconversion material where *one* higher energy visible (blue-green) photon is "cut" into *two* lower-energy near-infrared photons that both can be used by the solar cell. Here the efficiency of downconversion for the $(Nd^{3+},Yb^{3+})$ couple in $YF_3$ is studied to investigate if efficient two-step energy transfer occurs from the $^4G_{9/2}$ level of $Nd^{3+}$ (situated around 21 000 $cm^{-1}$ or 470 nm) exciting two neighboring $Yb^{3+}$ ions to the $^2F_{5/2}$ level (around 10 000 $cm^{-1}$ or 1000 nm). Optical measurements of $YF_3$ doped with $Nd^{3+}$ and $Yb^{3+}$ show that there is efficient energy transfer from $Nd^{3+}$ to $Yb^{3+}$, but downconversion from the $^4G_{9/2}$ level does not occur due to fast multiphonon relaxation. Relaxation from this level to lower-energy levels populates the $^4F_{3/2}$ level of $Nd^{3+}$ from which efficient one-step energy transfer to $Yb^{3+}$ occurs. Analysis of the luminescence decay curves for different $Yb^{3+}$-concentrations using Monte Carlo simulations reveals a high nearest neighbor transfer rate ($3.3\times10^5$ $s^{-1}$) through a dipole-dipole interaction mechanism. Downconversion is observed from the $^4D_{3/2}$ level (situated in the UV, around 28 000 $cm^{-1}$ or 360 nm) with an estimated quantum efficiency up to 140%. For application in solar cells this UV to 2 NIR downconversion will only result in a marginal reduction of spectral mismatch losses.

DOI: 10.1103/PhysRevB.81.035107 PACS number(s): 33.50.−j, 78.40.Ha, 78.47.−p, 78.55.Hx

## I. INTRODUCTION

The theoretical maximum conversion efficiency of solar cells is 30%.[1] A large part of the energy losses that limit the efficiency is related to the spectral mismatch: photons with energy smaller than the band-gap ($E_g$) will not be absorbed (sub-band-gap transmission) and a large part of the energy of photons with energy larger than the band gap is lost as heat (thermalization losses). There are two ways to reduce the energy losses related to the spectral mismatch: either the solar cell can be adapted to use the solar spectrum more efficiently, or the solar spectrum can be adapted before it is absorbed by the solar cell. Solar cells can be adapted to make better use of the spectrum by combining multiple semiconductor materials with different band gaps, each converting a different part of the solar spectrum with high efficiency. This approach has been successfully applied in tandem solar cells, and energy efficiencies over 40% have been reported.[2]

There are two ways to adapt the solar spectrum before it is absorbed by the solar cell. The first option is to add two lower-energy photons (that are otherwise transmitted) to obtain one higher energy photon that can be absorbed by the solar cell. This process is known as upconversion (UC) and is especially useful for solar cells with a large band-gap where transmission losses dominate. The second option is to split one higher energy photon to obtain two photons with a smaller energy. Each of these photons can subsequently be absorbed by the solar cell and generate an electron-hole pair. This is known as downconversion (DC) and is most beneficial for solar cells with a smaller band-gap where thermalization losses are the major loss factor. This process is also known as quantum cutting because one photon is "cut" into two smaller energy photons. Lanthanide ions are very well suited to use for both DC and UC because they have a rich energy level structure that allows for efficient spectral conversion. There are many examples of efficient upconversion and downconversion using lanthanides, either with one type of lanthanide ion or a pair of lanthanide ions.[3,4]

The effect of using either upconversion or downconversion materials in combination with solar cells has been modeled by Trupke *et al.*[5–7] When a solar cell with a band gap of 1.1 eV is combined with an ideal downconverting material in front of the cell (splitting every photon above $2E_g$ into two photons that can be absorbed and both generate an electron-hole pair), an efficiency of 40% is possible.[5] An upper limit of approximately 50% can be reached when a solar cell with a band gap of ~2 eV is combined with an ideal upconverter at the rear of the cell.[6,7] UC is a nonlinear process: for the two-step UC process (where two photons are added to obtain one photon with a larger energy) the UC light intensity $I_{UC}$ is proportional to square of the incident light intensity $I_i$. As a result, high conversion efficiencies are only obtained at sufficiently high excitation density which can be easily realized using lasers, but will require strong concentration of sunlight.

The most efficient UC is realized using lanthanide ions.[3] An example of a particularly efficient upconverting couple is $(Er^{3+},Yb^{3+})$. Under high power laser excitation an efficiency of around 50% has been reported for the conversion of NIR (~1000 nm) to visible light in $NaYF_4:Er^{3+}$, $Yb^{3+}$.[8] Gibart *et al.* proposed using this upconversion couple to increase the efficiency of a substrate-free GaAs solar cell and have reported an efficiency of 2.5% for excitation with 1.39 eV photons.[9] The feasibility of upconversion for solar cells was

 

also demonstrated using NIR upconversion in $NaYF_4$ doped with $Er^{3+}$.[7,10]

Contrary to UC, DC is a linear process. This makes it possible to obtain high conversion efficiencies independent of the incident power and allows for the use nonconcentrated sunlight. Demonstrations of efficient DC materials are still limited (contrary to UC materials). Initially the work focused on the conversion of a single VUV photon into two visible photons. The $(Gd^{3+},Eu^{3+})$ couple in a $LiGdF_4$ host lattice shows efficient VUV to VIS DC (internal quantum efficiency of approximately 190%) and $Er^{3+}$, $Gd^{3+}$, and $Tb^{3+}$ in the same host lattice have an efficiency of 130%.[4,11,12]

Downconversion of UV or visible photons into NIR photons was first demonstrated in $(Y,Yb)PO_4:Tb^{3+}$.[13] After excitation into the $^5D_4$ state of the $Tb^{3+}$-ion two neighboring $Yb^{3+}$ ions are excited through a cooperative energy transfer process. The $^5D_4$ level of $Tb^{3+}$ is found at about twice the energy of the $Yb^{3+}$ $^2F_{5/2}$ level, and after energy transfer $Yb^{3+}$ emission is observed around 1000 nm. This is just above the band gap of crystalline silicon which makes $Yb^{3+}$ an attractive candidate for DC materials to be used in combination with c-Si solar cells. More recently, cooperative downconversion has also been reported for $(Tb^{3+},Yb^{3+})$ in other host materials[14,15] and with other lanthanide couples, viz. $(Pr^{3+},Yb^{3+})$ (Ref. 16) and $(Tm^{3+},Yb^{3+})$.[17] It is not clear, however, that the second-order cooperative energy transfer process is the operative mechanism in the latter two systems, as also first-order energy transfer processes are possible and are expected to dominate.[18] Second-order cooperative energy transfer processes have a lower efficiency, making it only efficient at very high $Yb^{3+}$ concentrations where the $Yb^{3+}$ emission is largely quenched through concentration quenching. For more efficient energy transfer, an intermediate level on the donor ion should be used in order to obtain downconversion through two resonant energy transfer steps.

In this paper we investigate if efficient downconversion is possible with the $(Nd^{3+},Yb^{3+})$ couple in $YF_3$. We have chosen $YF_3$ as a host because this lattice has a low phonon energy (maximum phonon energy $\sim 500$ $cm^{-1}$) (Ref. 19); a lower phonon energy minimizes multiphonon relaxation processes between the closely spaced energy levels of $Nd^{3+}$, which can reduce the radiative downconversion efficiency. In Fig. 1 the downconversion scheme for the $(Nd^{3+},Yb^{3+})$ couple via sequential two-step energy transfer is shown. When $Nd^{3+}$ is excited into the $^4G_{9/2}$ state, part of the energy is transferred to $Yb^{3+}$ via cross relaxation: $Nd^{3+}$ $(^4G_{9/2} \rightarrow {}^4F_{3/2})$, $Yb^{3+}$ $(^2F_{7/2} \rightarrow {}^2F_{5/2})$, populating the $^2F_{5/2}$ level of $Yb^{3+}$. In a second step the remaining energy can be transferred to a second $Yb^{3+}$ ion, which can then emit a photon, or otherwise emission can occur from the $^4F_{3/2}$ level of $Nd^{3+}$.

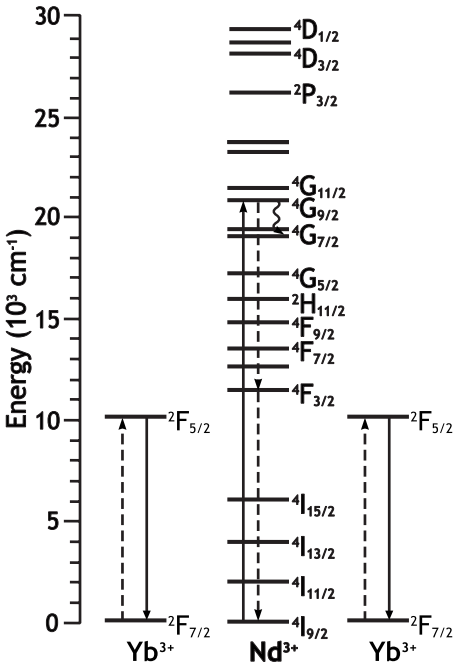


FIG. 1. Schematic representation of the desired mechanism for downconversion with the $Nd^{3+}$, $Yb^{3+}$ couple. $Nd^{3+}$ is excited into the $^4G_{9/2}$ state. Part of the energy is transferred to $Yb^{3+}$ via cross relaxation: $Nd^{3+}$ $(^4G_{9/2} \rightarrow {}^4F_{3/2})$, $Yb^{3+}$ $(^2F_{7/2} \rightarrow {}^2F_{5/2})$, populating the $^2F_{5/2}$ level of $Yb^{3+}$. In the second step the remaining energy can be transferred to a second $Yb^{3+}$ ion from the $^4F_{3/2}$ level of $Nd^{3+}$. Both $Yb^{3+}$ ions can then emit a photon of approximately 1000 nm.

## II. METHODS

### A. Synthesis

Crystalline powder samples of $YF_3$ doped with $Nd^{3+}$ and $Yb^{3+}$ were synthesized via coprecipitation. The $Nd^{3+}$ concentration was kept constant at 0.5% while the $Yb^{3+}$ concentration was varied between 0 and 10% (0, 2, 3, 5, or 10%). Also two samples without $Nd^{3+}$ were synthesized, containing 2% and 10% $Yb^{3+}$. In all cases the percentages given for the dopants $Yb^{3+}$ or $Nd^{3+}$ are in mol % with respect to $Y^{3+}$. A low $Nd^{3+}$ concentration was used to prevent cross relaxation between $Nd^{3+}$ pairs. The $Yb^{3+}$ concentration was varied: at low $Yb^{3+}$ concentrations there is less concentration quenching, while at higher concentrations energy transfer from $Nd^{3+}$ to $Yb^{3+}$ is more efficient because each $Nd^{3+}$ ion has one or more $Yb^{3+}$ neighbors. Therefore it is important to find the optimum $Yb^{3+}$ concentration. The samples were prepared by mixing stoichiometric amounts of $Y_2O_3$, $Nd_2O_3$, and $Yb_2O_3$ (purity at least 4N). The powder mixture was dissolved in dilute hydrochloric or nitric acid. After adding a solution with an excess of $NH_4F$ (98+%) a precipitate was formed, which was centrifuge-washed and then dried. The blend was put into an alumina crucible and fired in an oven together with an excess of $NH_4F$ under a nitrogen flow. The samples were first heated to 300 °C for 2 h (to remove adsorbed water molecules) and then to 1000 °C for 3 h. After the samples had cooled sufficiently they were crushed with a pestle and mortar and x-ray diffraction measurements were performed to check for phase purity.

### B. Measurements

Diffuse reflectance spectra were measured with a Perkin-Elmer Lambda 950 UV/VIS/IR absorption spectrometer. Emission and excitation measurements were performed using an Edinburgh Instruments FLS920 fluorescence spectrometer. The 0.3 m excitation double monochromator dis-

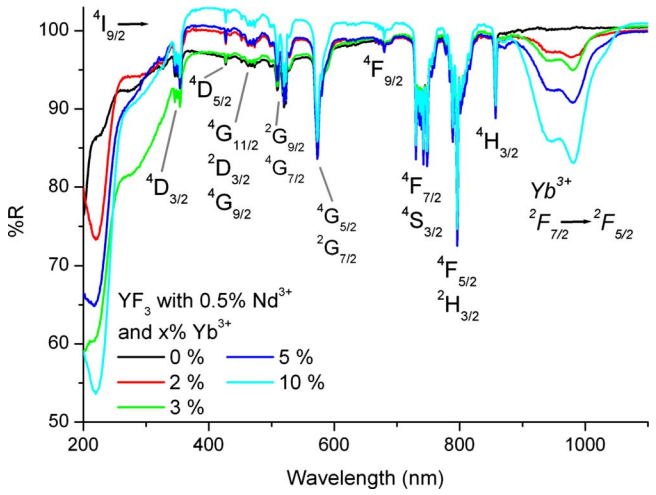


FIG. 2. (Color online) Diffuse reflectance spectra for $YF_3$:$Nd^{3+}$(0.5%), $Yb^{3+}$ (0, 2, 3, 5, and 10%).

perses light from a 450 W Xe lamp with gratings blazed at 300, 500, or 1200 nm. UV and visible sample emission is detected with an emission monochromator with a grating blazed at 300 or 500 nm and a Hamamatsu R928 photomultiplier tube (PMT). The NIR emission is detected with another emission monochromator with a grating blazed at 1200 nm and a liquid nitrogen-cooled Hamamatsu R5509–72 PMT. The Edinburgh fluorescence spectrometer is equipped with an Oxford helium flow cryostat for low temperature measurements. The spectra were not corrected for the instrumental response.

Lifetime measurements upon pulsed excitation at a wavelength of 452 nm were performed with the use of a Lambda Physik LPD3000 tunable dye laser with a Coumarin 120 dye solution (tunable between 423–462 nm). Lifetime measurements with an excitation wavelength of 950 nm were performed on the same setup with Styryl 14 dye solution (tunable between 904–992 nm). The dye laser is pumped by a Lambda Physik LPX100 excimer (XeCl) laser. The typical pulse width for the setup is ~20 ns and the repetition rate is 10 Hz. The laser excitation is steered into the sample chamber of the Edinburgh fluorescence spectrometer using a pair of prisms.

## III. RESULTS AND DISCUSSION

### A. Characterization

For all samples ($YF_3$ doped with 0.5% $Nd^{3+}$ and 0, 2, 3, 5, and 10% $Yb^{3+}$ and two samples doped with 2% and 10% $Yb^{3+}$) the x-ray diffraction patterns are consistent with the orthorhombic structure of $YF_3$. To monitor the incorporation of $Nd^{3+}$ and $Yb^{3+}$ in $YF_3$, diffuse reflection spectra were recorded. In the diffuse reflectance spectra (Fig. 2), it can be seen that the absorption strengths for the peaks corresponding to $Nd^{3+}$ absorptions (e.g., the $^4I_{9/2} \rightarrow {}^4F_{7/2}$ transition around 750 nm and the $^4I_{9/2} \rightarrow {}^4G_{9/2}$ transition around 500 nm) are very similar for all samples. This shows that the $Nd^{3+}$ was built into the lattice equally well for all samples, since in the starting mixture the same amount of $Nd^{3+}$(0.5%) was present. Furthermore, the peak for the $Yb^{3+}$ absorption strength around 1000 nm varies in good agreement with the $Yb^{3+}$ concentration that was present in the starting mixture.

In the UV (between 250 and 300 nm), a strong absorption band can be observed which is probably related to defects, possibly involving oxygen impurities. The intensity for this band varies between samples, and it is strongest for the sample codoped with 0.5% $Nd^{3+}$ and 3% $Yb^{3+}$.

### B. Luminescence

The energy level diagram in Fig. 1 shows the desired downconversion scheme: starting from the $Nd^{3+}$ $^4G_{9/2}$ level around 21 000 $cm^{-1}$ cross relaxation with a neighboring $Yb^{3+}$ ion involves partial energy transfer, which results in $Nd^{3+}$ in the $^4F_{3/2}$ state and $Yb^{3+}$ in the $^2F_{5/2}$ state. In the next step (phonon-assisted) energy transfer from the $^4F_{3/2}$ level of $Nd^{3+}$ to a second $Yb^{3+}$ ion results in a second excited $Yb^{3+}$ ion, and both ions can emit a 980 nm photon. To investigate if downconversion according to this scheme occurs, emission spectra were first recorded for $YF_3$:$Nd^{3+}$ without $Yb^{3+}$.

For downconversion it is crucial that the starting level $^4G_{9/2}$ is sufficiently long lived to allow for energy transfer to a neighboring $Yb^{3+}$ ion. If the level has a sufficiently long lifetime, emission from the level can be observed and one can expect the occurrence of downconversion. However, the energy level diagram in Fig. 1 shows that a competing process, multiphonon relaxation from $^4G_{9/2}$ to the next lower level ($^2G_{9/2}$) is also possible which may prevent downconversion. If multiphonon relaxation to the next lower level dominates, the lifetime of the level is decreased and no emission will be observed, as it is unlikely that downconversion can compete with fast multiphonon relaxation. Downconversion from higher energy levels was also investigated. The energy level diagram in Fig. 1 reveals relatively large energy gaps below the $^2P_{3/2}$ and the $^4D_{3/2}$ level which indicates that these states may be sufficiently long lived to give rise to downconversion.

Figure 3 shows the room temperature emission spectra of $YF_3$ doped with 0.5% $Nd^{3+}$ for excitation in the $Nd^{3+}$ $^4D_{1/2}$ level (354 nm) and the $^4G_{9/2}$ level (464 nm). The results show that upon excitation at 354 nm, emission is observed from both the $^4D_{3/2}$ and the $^2P_{3/2}$ level to the $^4I_J$ level. This indicates that these levels may serve as starting levels for downconversion. Upon excitation at 464 nm, only infrared emission is observed around 870, 1050, and 1340 nm, all of which originate from $^4F_{3/2} \rightarrow {}^4I_J$ transitions. The absence of $^4G_{9/2} \rightarrow {}^4I_J$ emissions shows that the energy gap between the $^4G_{9/2}$ level and the next lower level ($^2G_{9/2}$) is bridged by fast multiphonon relaxation and that radiative decay from the $^4G_{9/2}$ level cannot compete with this nonradiative relaxation process. As a result downconversion from the $^4G_{9/2}$ level is probably not possible. The $^4F_{3/2} \rightarrow {}^4I_J$ emission peaks are also observed for excitation into the higher energy levels, such as the $^4D_{1/2}$, $^4D_{3/2}$, and the $^2P_{3/2}$ levels. This indicates that from the higher energy emitting levels nonradiative relaxation to the $^4F_{3/2}$ level also occurs. This is confirmed by the excitation spectrum of the $^4F_{3/2} \rightarrow {}^4I_{9/2}$ emission around 866 nm (Fig. 4) where peaks can be observed corresponding

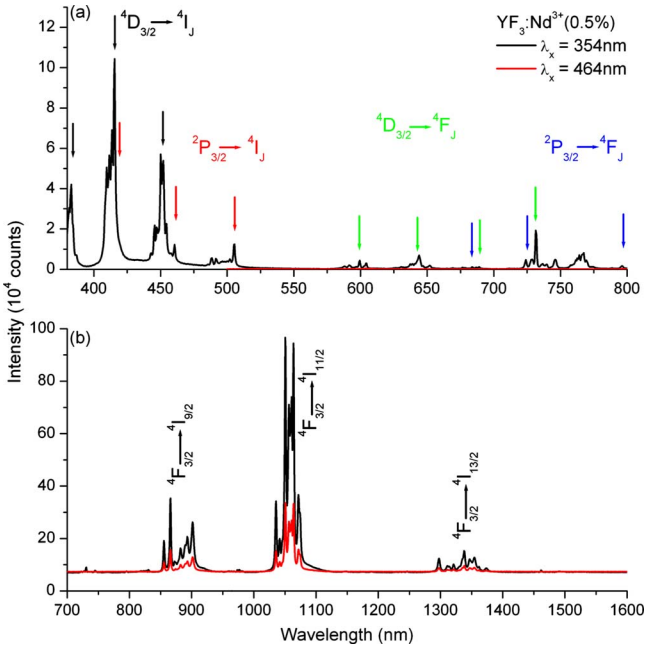


FIG. 3. (Color online) Room temperature emission spectra for the visible (a) and infrared (b) part of the spectrum for $YF_3:Nd^{3+}(0.5\%)$. The excitation wavelength is 354 nm ($^4D_{1/2}$ level).

to transitions to all levels above the $^4F_{3/2}$ level of $Nd^{3+}$.

The $Nd^{3+}$ emission is quenched when the samples are codoped with $Yb^{3+}$. At a concentration of 3% $Yb^{3+}$, the $Nd^{3+}$ emission both in the visible and in the infrared has almost completely disappeared (Fig. 5). When the $Yb^{3+}$ concentration is increased to 10% the remaining $Nd^{3+}$ emission intensity is less than 1% of the intensity for the sample without $Yb^{3+}$. At the same time, the $Yb^{3+}$ emission around 1000 nm starts to increase, and it reaches its maximum for the sample doped with 0.5% $Nd^{3+}$ and 5% $Yb^{3+}$. Increasing the concentration further does not lead to a higher $Yb^{3+}$ emission intensity. Instead, the emission intensity starts to decrease for the sample with 0.5% $Nd^{3+}$ and 10% $Yb^{3+}$, which is explained by concentration quenching.

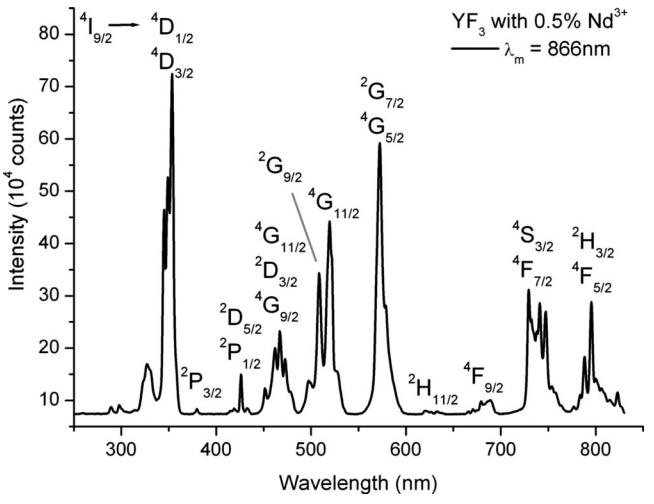


FIG. 4. Room temperature excitation spectrum of $^4F_{3/2} \rightarrow {}^4I_{9/2}$ emission (866 nm) for $YF_3:Nd^{3+}(0.5\%)$.

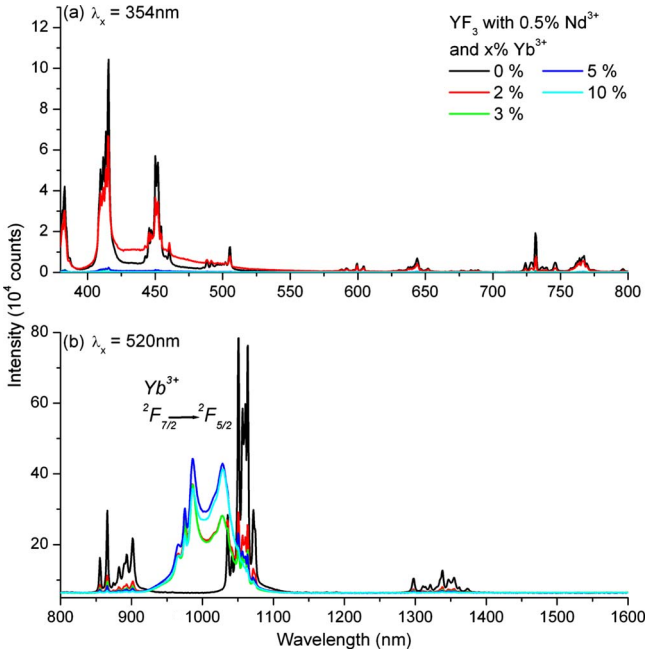


FIG. 5. (Color online) Room temperature emission spectra for $YF_3:Nd^{3+}(0.5\%)$, $Yb^{3+}$ (0, 2, 3, 5, and 10%). (a) Visible part of the spectrum, excitation wavelength is 354 nm ($^4D_{1/2}$ level). (b) Infrared part of the spectrum, excitation wavelength is 520 nm ($^4G_{11/2}$ level).

For the highest $Yb^{3+}$ concentration there is also a change in the relative intensities of the $Yb^{3+}$ emission at 986 and at 1028 nm. The peak at 986 nm is higher than the peak at 1028 nm for $Yb^{3+}$ concentrations up to 5%, while the 1028 nm peak is higher for the $YF_3:Nd^{3+}(0.5\%)$, $Yb^{3+}(10\%)$ sample. For this high concentration, reabsorption of the shorter wavelength emission around 986 nm can occur, thus lowering the relative intensity of this emission component. Furthermore, energy transfer over multiple $Yb^{3+}$ ions can occur to $Yb^{3+}$ ions that emit at lower-energy values, leading to emission at longer wavelengths.

The emission spectra recorded after excitation in the lower-energy levels of $Nd^{3+}$ (below the $^4G_{9/2}$ level), shown for $^4G_{11/2}$ (520 nm) in Fig. 5(b), demonstrate that the energy transfer from $Nd^{3+}$ to $Yb^{3+}$ after multiphonon relaxation is efficient and does lead to emission from $Yb^{3+}$ as desired. This indicates that one-step energy transfer occurs from $Nd^{3+}$ to $Yb^{3+}$. After nonradiative relaxation to the $^4F_{3/2}$ level, efficient transfer can be expected as the $^4F_{3/2} \rightarrow {}^4I_{11/2}$ transition on $Nd^{3+}$ is resonant with the $^2F_{5/2} \rightarrow {}^2F_{7/2}$ transition on $Yb^{3+}$.

To determine if downconversion occurs from the higher energy levels via the two-step energy transfer process (yielding two IR photons) excitation spectra were recorded for emission from the $^4F_{3/2}$ level of $Nd^{3+}$ in $YF_3:Nd^{3+}(0.5\%)$ and emission from the $^2F_{5/2}$ level of $Yb^{3+}$ in $YF_3:Nd^{3+}(0.5\%)$, $Yb^{3+}(2\%)$. If downconversion occurs from a high energy level, the relative intensity of the peak corresponding to the transition to this level should increase in the excitation spectrum of the $Yb^{3+}$ emission, as two instead of one IR photons are generated.[18] The spectra are compared by normalizing to the excitation of the $Nd^{3+}$ $^2G_{7/2}/{}^4G_{5/2}$ level (Fig. 6). Excitation below the $^2G_{7/2}/{}^4G_{5/2}$ level will be fol-

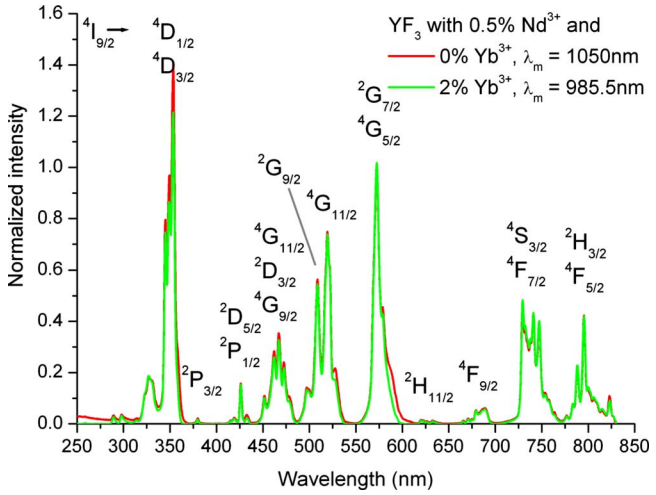


FIG. 6. (Color online) Room temperature excitation spectrum of $Nd^{3+}$ emission (1050 nm) in $YF_3$:$Nd^{3+}$(0.5%) and $Yb^{3+}$ emission (986 nm) in $YF_3$:$Nd^{3+}$(0.5%), $Yb^{3+}$(2%), both normalized at 572 nm ($^2G_{7/2}$/$^4G_{5/2}$).

lowed by rapid multiphonon relaxation to the $^4F_{3/2}$ level as is evident from the small energy gaps separating the levels below this level (see Fig. 1). In both excitation spectra the peaks for these levels will appear with approximately the same relative intensities. Figure 6 shows that there is no increase in the relative intensity of the peak for excitation into the $^4G_{9/2}$ level (470 nm) for the $Yb^{3+}$ codoped sample compared to the sample only doped with $Nd^{3+}$. This indicates that downconversion does not occur from the $^4G_{9/2}$ level. There is, however, an increase in the relative intensity of the peak for excitation into the $^4D_{3/2}$ level at 354 nm. When comparing the excitation peak intensities of the 866 nm $Nd^{3+}$ and the 986 nm $Yb^{3+}$ emission, an increase is observed in all samples codoped with $Yb^{3+}$ (Fig. 7). The ratio of the intensities of the $^4D_{3/2}$ excitation peak relative to the $^2G_{7/2}$/$^4G_{5/2}$ excitation peaks increases from 1.1 to 1.4 when the $Yb^{3+}$ concentration is increased from 2 to 10%. This indicates that downconversion occurs from the $Nd^{3+}$ $^4D_{3/2}$ level, and that the efficiency increases with increasing $Yb^{3+}$ concentration,

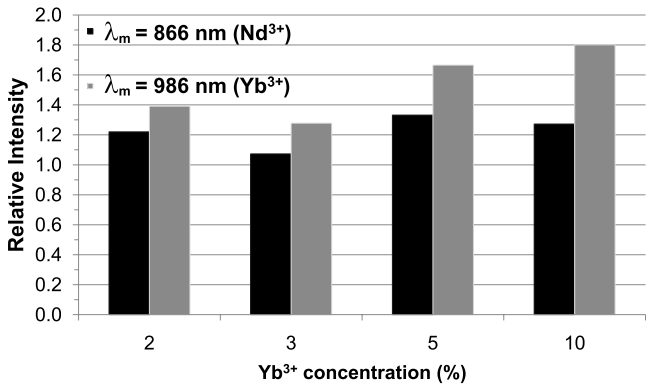


FIG. 7. Comparison of relative excitation peak intensities of $Nd^{3+}$ and $Yb^{3+}$ emission for $YF_3$:$Nd^{3+}$(0.5%), $Yb^{3+}$ (2, 3, 5, and 10%). The excitation spectra were measured at room temperature and normalized at 572 nm.

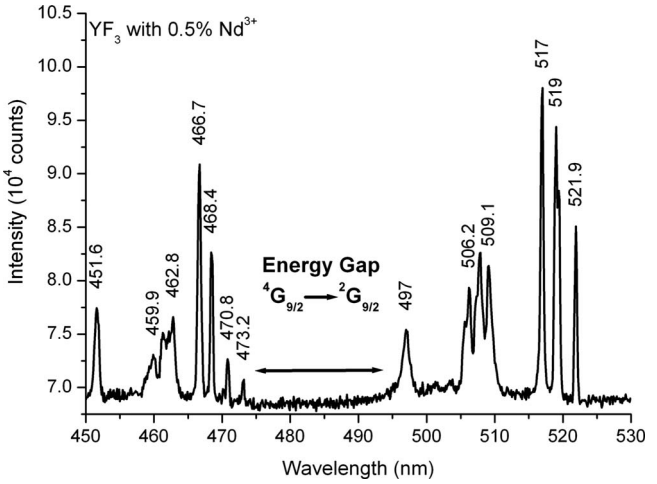


FIG. 8. High resolution excitation spectrum of 1050 nm emission in $YF_3$:$Nd^{3+}$(0.5%) measured at 4 K.

as expected. Based on the observed intensity ratios, it can be concluded that the downconversion efficiency increases up to 140% in the sample with 10% $Yb^{3+}$.

The absence of downconversion from the $^4G_{9/2}$ level is attributed to multiphonon relaxation. To further investigate the multiphonon relaxation process, a high resolution excitation spectrum of the $^4F_{3/2}$ emission in $YF_3$:$Nd^{3+}$(0.5%) was recorded to determine the energy gap between the $^4G_{9/2}$ and $^2G_{9/2}$ level (Fig. 8). The excitation spectrum shows sharp transitions to the various crystal field (CF) components of the $^4G_{9/2}$ level between 460 and 475 nm and to the $^2G_{9/2}$ components between 495 and 525 nm. The energy gap between the lowest CF of the $^4G_{9/2}$ and the highest CF component of the $^2G_{9/2}$ level is determined to be 1012 $cm^{-1}$. Since the maximum phonon energy of $YF_3$ is ~500 $cm^{-1}$, the energy gap between the $^4G_{9/2}$ and $^2G_{9/2}$ level can be bridged by two to three phonons. Based on the energy-gap law and experimental results, a rule of thumb predicts that radiative decay and multiphonon relaxation can compete when the gap is five times the phonon energy. For a smaller energy-gap, multiphonon relaxation dominates. Therefore the absence of emission from the $Nd^{3+}$ $^4G_{9/2}$ level is in agreement with present findings: the energy difference between the $^4G_{9/2}$ level and the next lower level ($^2G_{9/2}$) is small enough for nonradiative decay to dominate in this host, making DC from the $^4G_{9/2}$ level inefficient. In hosts with a smaller phonon energy, e.g., chlorides ($\hbar\omega \sim 250$ $cm^{-1}$) or bromides ($\hbar\omega \sim 180$ $cm^{-1}$), DC from the $^4G_{9/2}$ level may compete with nonradiative relaxation, and efficient downconversion could be achieved.

### C. Decay measurements

To gain further insight in the energy transfer processes between $Nd^{3+}$ and $Yb^{3+}$, luminescence decay curves were recorded for the $Nd^{3+}$ and $Yb^{3+}$ emission upon excitation into the $^4G_{9/2}$ level at 456 nm (Figs. 9 and 10). The luminescence decay curves of the $Nd^{3+}$ $^4F_{3/2}$ emission (866 nm) in $YF_3$:$Nd^{3+}$(0.5%) can be described by a single exponential with a lifetime of 390 $\mu$s. When the sample is codoped with

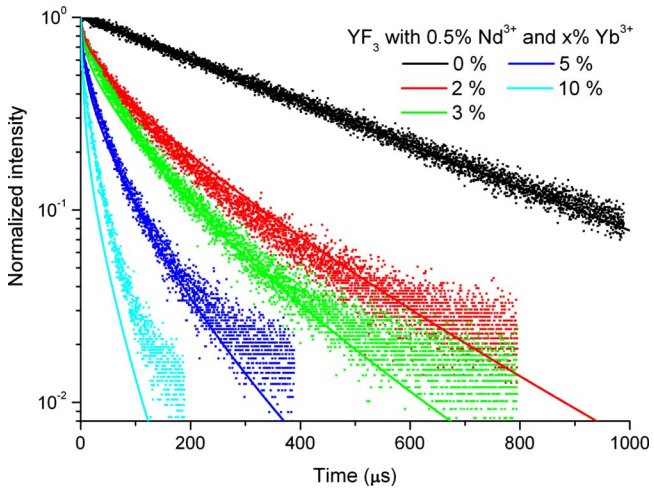


FIG. 9. (Color online) Room temperature lifetime measurements (dotted lines) of $Nd^{3+}$ $^4F_{3/2}$ emission (866 nm) in $YF_3:Nd^{3+}(0.5\%)$ codoped with $Yb^{3+}$ (0, 2, 3, 5, and 10%) after excitation into the $Nd^{3+}$ $^4G_{9/2}$ level at 456 nm. The solid lines are simulated curves using model for single-step energy transfer through dipole-dipole interaction [Eqs. (1)–(3)].

$Yb^{3+}$, the lifetime decreases and the decay is no longer single exponential (Fig. 9). This shows that energy transfer from $Nd^{3+}$ to $Yb^{3+}$ occurs and the transfer rate increases as the $Yb^{3+}$ concentration is raised. The nonexponential character of the decay curves reflects the different distributions of $Yb^{3+}$ ions around different $Nd^{3+}$ ions, which gives rise to a wide distribution of transfer rates between $Nd^{3+}$ and $Yb^{3+}$ ions. The rapid decrease of the decay time upon raising the $Yb^{3+}$ concentration from 2 to 10% shows that energy transfer from $Nd^{3+}$ to $Yb^{3+}$ is efficient, consistent with the rapid drop of the $Nd^{3+}$-emission intensity upon adding $Yb^{3+}$ observed in Fig. 5. To analyze the energy transfer more quantitatively, the luminescence decay curves were modeled using Monte Carlo simulations. In a previous paper the basics of the modeling

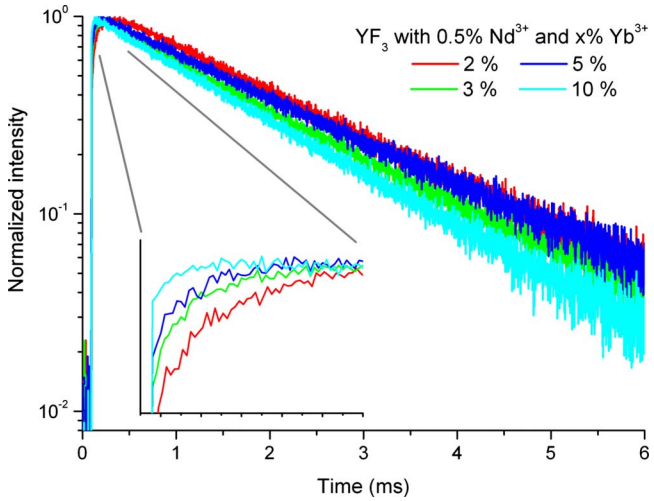


FIG. 10. (Color online) Room temperature lifetime measurements of $Yb^{3+}$ $^2F_{5/2}$ emission (986 nm) in $YF_3:Nd^{3+}(0.5\%)$, $Yb^{3+}$ (2, 3, 5, and 10%) after excitation into the $Nd^{3+}$ $^4G_{9/2}$ level at 456 nm. The inset shows the buildup in the first 0.2 ms of the curve.

procedure have been outlined and the model was used to distinguish between different possible energy transfer mechanisms (cooperative, accretive or phonon-assisted single step).[13] The present energy transfer process clearly involves a single-step transfer from $Nd^{3+}$ to neighboring $Yb^{3+}$ ions and only this mechanism is therefore considered. For the single-step energy transfer through dipole-dipole interaction, the transfer rate to all neighbors is given by

$$\gamma_{tr} = C_{tr} \sum_i 1/r_i^6, \tag{1}$$

where $\gamma_{tr}$ is the transfer rate for a $Nd^{3+}$ ion in the excited $^4F_{3/2}$ state to transfer to all neighboring $Yb^{3+}$ ions at distances $r_i$. The constant $C_{tr}$ is fitted to the measured intensity for the sample codoped with 2% $Yb^{3+}$ and the summation is over all $Yb^{3+}$ neighbors $i$. A discrete atom model was used based on the unit cell of $YF_3$ (orthorhombic with $a=6.353$ Å, $b=6.850$ Å, and $c=4.393$ Å) and the coordinates of the Y atoms in the unit cell.[20,21] The size of the box considered for energy transfer was $5^3$ unit cells which means that all interactions up to 15 Å were taken into account. For larger distances no improvement of the simulations was observed indicating that energy transfer over longer distances does not contribute significantly. The lattice sites were filled randomly with $Y^{3+}$ or $Yb^{3+}$ with a probability specified by the $Y^{3+}$ to $Yb^{3+}$ ratio. Substitution of one of the lanthanides by $Nd^{3+}$ generated a particular configuration. For each configuration the single exponential decay curve is given by

$$I(t) = e^{-t(\gamma_{tr}+\gamma_r)}, \tag{2}$$

where $t$ is time, $\gamma_r$ is the radiative decay rate of the $^4F_{3/2}$ state of $Nd^{3+}$ in $YF_3$ and $\gamma_{tr}$ is the energy transfer rate as calculated with Eq. (1). The decay curves recorded result from an ensemble average of configurations. Therefore an ensemble average signal was calculated,

$$\langle I(t) \rangle = \langle e^{-t(\gamma_{tr}+\gamma_r)} \rangle, \tag{3}$$

where $\langle\ \rangle$ denotes ensemble averaging over 10 000 configurations. With this number convergence was reached. The simulations are shown in Fig. 9 for the different $Yb^{3+}$ concentrations for $\gamma_r = 2.55 \times 10^3$ $s^{-1}$ ($\tau_r = 390$ $\mu$s) and $C_{tr} = 7.07 \times 10^8$ Å$^6$ $ms^{-1}$. The agreement is excellent showing that the energy transfer between $Nd^{3+}$ and $Yb^{3+}$ is well described by energy transfer through dipole-dipole interactions. The energy transfer is indeed very efficient. The transfer rate to nearest neighbors at 3.6 Å is $3.25 \times 10^5$ $s^{-1}$, more than 100 times faster than the radiative decay rate of $2.55 \times 10^3$ $s^{-1}$.

In the decay curves of the $Yb^{3+}$ emission, a buildup is observed in the first part of the curve (Fig. 10), causing the $Yb^{3+}$ emission to reach a maximum approximately 150 $\mu$s after the start of the measurement. This buildup time is similar to the decay times of the $^4F_{3/2}$ emission from $Nd^{3+}$, which confirms that the $Yb^{3+}$ emission is fed by energy transfer from the $Nd^{3+}$ $^4F_{3/2}$ level. The buildup time decreases from 80 $\mu$s for $YF_3:Nd^{3+}(0.5\%)$, $Yb^{3+}(2\%)$ to 13 $\mu$s for $YF_3:Nd^{3+}(0.5\%)$, $Yb^{3+}(10\%)$, confirming that the energy transfer becomes more efficient at higher $Yb^{3+}$ concentrations. The effect of concentration quenching can be seen in

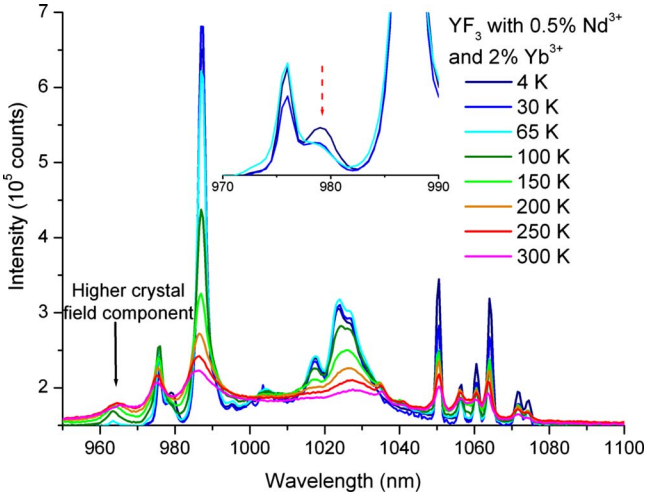


FIG. 11. (Color online) Temperature dependent emission spectra for $YF_3$:$Nd^{3+}$(0.5%), $Yb^{3+}$(2%). The inset shows the effect of temperature on the peak at 980 nm.

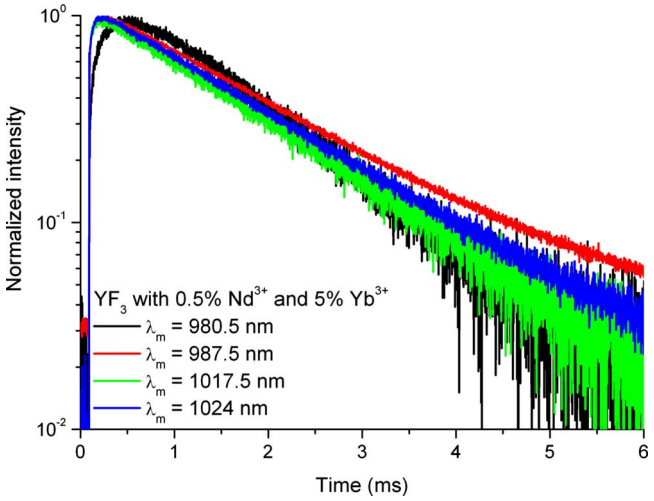


FIG. 12. (Color online) Lifetime measurements at 4 K of $Yb^{3+}$ $^2F_{5/2}$ emission at different wavelengths in $YF_3$:$Nd^{3+}$(0.5%), $Yb^{3+}$(5%) after excitation into the $Nd^{3+}$ $^4G_{9/2}$ level at 456 nm.

the long time part of the decay curve: at low $Yb^{3+}$ concentrations the lifetime is approximately 1900 $\mu$s, and as the $Yb^{3+}$ concentration increases to 10%, the lifetime decreases to ~1560 $\mu$s. The decrease in lifetime is ascribed to energy migration of the excitation energy over the $Yb^{3+}$ sublattice, which can result in quenching of the luminescence if the migrating excitation encounters a quenching site.

### D. Temperature dependent measurements

To gain further understanding about the energy transfer processes and the concentration quenching in $YF_3$:$Nd^{3+}$, $Yb^{3+}$, temperature dependent measurements were performed. Figure 11 shows typical temperature-dependent spectra for $YF_3$:$Nd^{3+}$(0.5%), $Yb^{3+}$(2%). At 4 K the emission peaks of both $Nd^{3+}$ and $Yb^{3+}$ are very narrow compared to the spectra at room temperature. Thermally induced relaxation processes cause the emission peaks to broaden at higher temperatures (lifetime broadening). Furthermore, additional peaks for emission from higher crystal field components start to appear when the temperature is raised. An example of this effect is the peak for emission from a higher crystal field component of the $Yb^{3+}$ $^2F_{5/2}$ level at 965 nm that appears when the temperature is increased to 50 K.

As seen from the room temperature emission spectra (Fig. 5) and the lifetime measurements of the $Yb^{3+}$ emission (Fig. 10) $Yb^{3+}$ $^2F_{5/2}$ emission starts to decrease due to concentration quenching for high $Yb^{3+}$ concentrations. At very low temperatures (4 K), concentration quenching is hampered, which causes a strong increase in the $Yb^{3+}$ emission intensity. This is explained by the small energy mismatches between the energy levels of neighboring $Yb^{3+}$ ions, which impose the need for phonon-assisted energy transfer; by freezing out the phonons at low temperatures, the energy migration becomes less efficient and the concentration quenching is reduced.

At low temperatures, an additional peak is visible in the $Yb^{3+}$ emission spectra at 980.5 nm (see the inset of Fig. 11), which disappears when the temperature is raised above 50 K. Low-temperature lifetime measurements for the emission peaks between 980 and 1024 nm are compared (Fig. 12). The lifetime of the tail of the decay curves is approximately 1500 $\mu$s for all curves, and all four decay curves show a buildup in the beginning of the curve. The buildup time is ~50 $\mu$s for emission wavelengths between 987 and 1024 nm, and is attributed to energy transfer from $Nd^{3+}$ to $Yb^{3+}$ (see also Fig. 10). The buildup time for the 980.5 nm emission is approximately 225 $\mu$s. The longer buildup time on the decay curve and the observation that this emission peak disappears above 50 K can be explained by the presence of a small amount of oxygen in the sample. For $Yb^{3+}$ ions situated next to an oxygen impurity, a very common contamination in fluorides, the lowest $^2F_{5/2}$ level is lowered in energy (~47 $cm^{-1}$ based on the position of the emission lines at 976 nm for $Yb^{3+}$ on the dominant site, and 980.5 nm for $Yb^{3+}$ next to an oxygen impurity, which will be indicated by Yb-$O_F'$). At higher temperatures thermal detrapping occurs, and this explains the observed decrease in the 980.5 nm emission intensity above 50 K. To confirm the presence of Yb-$O_F'$, the excitation spectrum for the 980.5 nm emission was compared to an excitation spectrum of $Yb^{3+}$ emission at 987 nm [Fig. 13(a)]. In the excitation spectrum for the $Yb^{3+}$ emission (solid line) peaks for excitation into the different $Nd^{3+}$ levels are present (compare Fig. 6), while for the 980.5 nm emission (dotted line) a broad band between 250 and 350 nm can be observed. Such a band is typical for oxygen ligand-to-metal charge-transfer (CT) for lanthanides, in this case from $O^{2-}$ to $Yb^{3+}$.[22] This is further confirmed by comparing the emission spectra for excitation into the CT band which results in an intense $Yb^{3+}$ emission at 980.5 nm, while for excitation into the $Nd^{3+}$ $^4G_{9/2}$ level the intrinsic $Yb^{3+}$ emission lines dominate [Fig. 13(b)]. The shift of the emission peak indicates that oxygen lowers the position of the $Yb^{3+}$ $^2F_{5/2}$ energy level, which can then act as an energy trap (Yb-$O_F'$) at lower temperatures, resulting in an emission peak at 980 nm below 50 K (Fig. 11). The slower buildup in the decay curve of the 980 nm emission is then explained by energy transfer to Yb-$O_F'$ (Fig. 12).

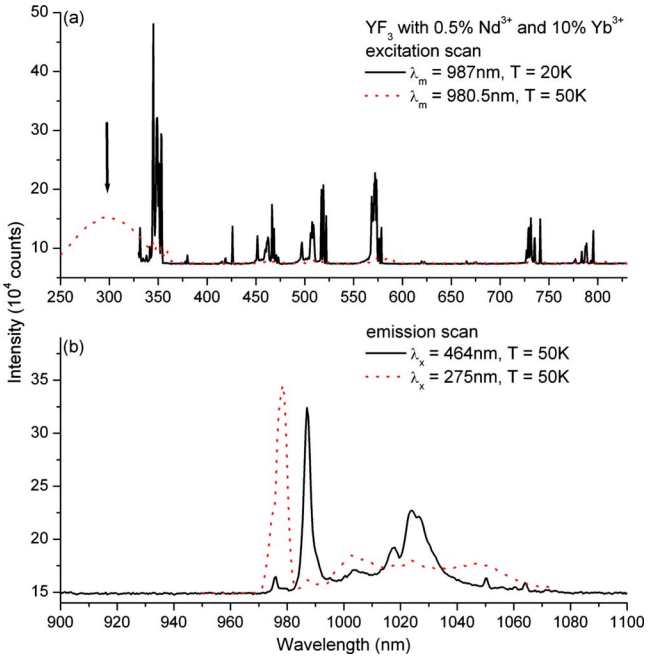


FIG. 13. (Color online) Excitation (a) and emission (b) spectra for $YF_3:Nd^{3+}(0.5\%)$, $Yb^{3+}(10\%)$ showing the $O^{2-}$-$Yb^{3+}$ CT band and emission from $Yb^{3+}$ affected by the presence of oxygen ($Yb\text{-}O_F'$).

The presence of oxygen can also be observed in the absorption spectra as an absorption band around 250 nm (Fig. 2). Oxygen and fluoride have a similar ionic radius, making oxide contamination of fluorides a commonly observed problem.

## IV. CONCLUSIONS

Downconversion for the $(Nd^{3+}, Yb^{3+})$ couple has been investigated in $YF_3:Nd^{3+}$, $Yb^{3+}$. Emission and excitation measurements of $YF_3:Nd^{3+}(0.5\%)$ show that excitation into energy levels of $Nd^{3+}$ between 28 500 and 17 500 $cm^{-1}$ (350–570 nm), results in nonradiative decay to the $^4F_{3/2}$ level, followed by emission from this level to the $^4I_J$ levels in the infrared. In codoped samples downconversion from the $Nd^{3+}$ $^4G_{9/2}$ level via the cross-relaxation process $Nd^{3+}$ ($^4G_{9/2} \rightarrow {}^4F_{3/2}$), $Yb^{3+}$ ($^2F_{7/2} \rightarrow {}^2F_{5/2}$), followed by a second energy transfer step from the $^4F_{3/2}$ level of $Nd^{3+}$ to $Yb^{3+}$, could possibly lead to the emission of two IR photons from $Yb^{3+}$. However, fast multiphonon relaxation is found to occur from the $^4G_{9/2}$ level to the lower $^2G_{9/2}$ level and this prevents efficient downconversion from the $^4G_{9/2}$ level, as cross-relaxation is much less efficient than multiphonon relaxation.

The multiphonon relaxation from the $^4G_{9/2}$ level and lower-energy levels results in population of the $^4F_{3/2}$ level of $Nd^{3+}$. From here efficient one-step energy transfer to $Yb^{3+}$ occurs through dipole-dipole interaction. The energy difference between the $Nd^{3+}$ $^4G_{9/2}$ and the next lower $^2G_{9/2}$ level is determined to be 1012 $cm^{-1}$ and this small energy difference explains that multiphonon relaxation dominates in $YF_3$, where the maximum phonon energy is around 500 $cm^{-1}$. Possibly efficient downconversion from the $Nd^{3+}$ $^4G_{9/2}$ level to two $Yb^{3+}$ ions can be achieved in a host lattice with much lower phonon energies (e.g., bromides or chlorides).

From the higher energy $^4D_{3/2}$ level of $Nd^{3+}$ downconversion is observed with efficiencies up to 40%. The high energy position of this level (in the UV part of the spectrum) does not make this a promising downconversion route for solar cell applications.

## ACKNOWLEDGMENTS

This work is part of the Joint Solar Programme (JSP) of the Stichting voor Fundamenteel Onderzoek der Materie FOM, which is supported financially by Nederlandse Organisatie voor Wetenschappelijk Onderzoek (NWO). The JSP is cofinanced by Gebied Chemische Wetenschappen of NWO and Stichting Shell Research. Financial support from the "Energie Onderzoek Subsidie" (EOS) program of SenterNovem, an agency of the "Ministerie van Economische Zaken" of the Netherlands, is gratefully acknowledged.

*a.meijerink@uu.nl

[1] W. Shockley and H. J. Queisser, J. Appl. Phys. **32**, 510 (1961).
[2] M. A. Green, K. Emery, Y. Hishikawa, and W. Warta, Prog. Photovoltaics **17**, 85 (2009).
[3] F. Auzel, Chem. Rev. **104**, 139 (2004).
[4] R. T. Wegh, H. Donker, K. D. Oskam, and A. Meijerink, Science **283**, 663 (1999).
[5] T. Trupke, M. A. Green, and P. Würfel, J. Appl. Phys. **92**, 1668 (2002).
[6] T. Trupke, M. A. Green, and P. Würfel, J. Appl. Phys. **92**, 4117 (2002).
[7] T. Trupke, A. Shalav, B. S. Richards, P. Würfel, and M. A. Green, Sol. Energy Mater. Sol. Cells **90**, 3327 (2006).
[8] J. F. Suyver, A. Aebischer, D. Biner, P. Gerner, J. Grimm, S. Heer, K. W. Krämer, C. Reinhard, and H. U. Güdel, Opt. Mater. **27**, 1111 (2005).
[9] P. Gibart, F. Auzel, J. C. Guillaume, and K. Zahraman, Jpn. J. Appl. Phys., Part 1 **35**, 4401 (1996).
[10] A. Shalav, B. S. Richards, T. Trupke, K. W. Krämer, and H. U. Güdel, Appl. Phys. Lett. **86**, 013505 (2005).
[11] K. D. Oskam, R. T. Wegh, H. Donker, E. V. D. van Loef, and A. Meijerink, J. Alloys Compd. **300-301**, 421 (2000).
[12] R. T. Wegh, E. V. D. van Loef, and A. Meijerink, J. Lumin. **90**, 111 (2000).
[13] P. Vergeer, T. J. H. Vlugt, M. H. F. Kox, M. I. den Hertog, J. P. J. M. van der Eerden, and A. Meijerink, Phys. Rev. B **71**, 014119 (2005).
[14] Q. Y. Zhang, G. F. Yang, and Z. H. Jiang, Appl. Phys. Lett. **91**, 051903 (2007).
[15] J. L. Yuan, X. Y. Zeng, J. T. Zhao, Z. J. Zhang, H. H. Chen, and

X. X. Yang, J. Phys. D **41**, 105406 (2008).
[16] G. Lakshminarayana, H. Yang, S. Ye, Y. Liu, and J. Qiu, J. Mater. Res. **23**, 3090 (2008).
[17] G. Lakshminarayana, H. Yang, S. Ye, Y. Liu, and J. Qiu, J. Phys. D **41**, 175111 (2008).
[18] B. M. van der Ende, L. Aarts, and A. Meijerink, Adv. Mater. **21**, 3073 (2009).
[19] H. E. Rast, H. H. Caspers, and S. A. Miller, Phys. Rev. **180**, 890 (1969).
[20] Ralph Walter Graystone Wyckoff, *Crystal Structures*, 2nd ed. (Interscience, New York, 1963), Vol. 2, p. 58–60.
[21] A. Zalkin and D. H. Templeton, J. Am. Chem. Soc. **75**, 2453 (1953).
[22] L. van Pieterson, M. Heeroma, E. de Heer, and A. Meijerink, J. Lumin. **91**, 177 (2000).